Fault Detection and Subsurface Model Based on Gravity Data in Pronojiwo, Lumajang, Indonesia

Laily Nur Hofi
Department of Physics, Faculty of Mathematics and Science, Brawijaya University

Maryanto, Sukir
Department of Physics, Faculty of Mathematics and Science, Brawijaya University

Susilo, Adi
Department of Physics, Faculty of Mathematics and Science, Brawijaya University

Andinisari, Ratri
Department of Civil Engineering, Malang National Institute of Technology

他

https://doi.org/10.5109/7236820

出版情報：Evergreen. 11 (3), pp.1666-1675, 2024-09. 九州大学グリーンテクノロジー研究教育センター
バージョン：

Fault Detection and Subsurface Model Based on Gravity Data in Pronojiwo, Lumajang, Indonesia

Laily Nur Hofi[1], Sukir Maryanto[1,2,*], Adi Susilo[1], Ratri Andinisari[3], Sri Dwi Wuryani[2]

[1]Department of Physics, Faculty of Mathematics and Science, Brawijaya University, Indonesia

[2]Brawijaya Volcanology and Geothermal Research Center, Brawijaya University, Indonesia

[3]Department of Civil Engineering, Malang National Institute of Technology, Indonesia

*Author to whom correspondence should be addressed:
E-mail: sukir@ub.ac.id

(Received August 29, 2023: Revised May 14, 2024: Accepted July 13, 2024).

Abstract: Understanding the subsurface structure is vital geophysical investigations, precisely local fault detection. Gravity anomalies were measured using satellite data from Global Gravity plus (GGMplus), and direct acquisition was used to achieve this goal. The residual anomalies range from -4.9 mGal to 3.6 mGal for the satellite and between -1.6 mGal to 0.94 mGal for direct acquisition. First Horizontal Derivative (FHD) and Second Vertical Derivative (SVD) analyses were performed based on the residual anomaly contrast. By integrating direct acquisition and GGMplus gravity data, this study aimed to analyze the existing local fault distribution in the research area. The preliminary result indicates the presence of faults with NW-SE orientation. Additionally, 2-D stratigraphic modeling includes three formations: andesitic lava, breccia, and tuff. The research provides a deeper understanding of subsurface structures using a combination of gravity data.

Keywords: Fault detection; subsurface structure; derivative analysis; gravity acquisition; GGMplus.

1. Introduction

The intersection between tectonic plates and plate discontinuities has the potential to generate faults[1,2]. These faults create zones with weak ground stability, triggering movements that manifest as earthquakes and landslides[3]. Based on synthesis documentation of Indonesia's seismotectonics, East Java is one of the provinces with a high risk of earthquakes, predominantly with magnitudes of 4.8 to 5.5. The subduction zone is part of the Sunda arc, where the Eurasian plate subducts orthogonally beneath the Indo-Australian plate[4,5]. In addition to the subduction zone, regional and local fault activities trigger earthquakes in the East Java region. Many faults in East Java still need to be accurately identified, and the Geological Agency's research is ongoing.

One of the unidentified active faults that became a source of loss of human life and significant infrastructure damage was the earthquake in Cianjur, which had a magnitude of 5.6[6]. Based on preliminary data from the Meteorology, Climatology, and Geophysics Agency (BMKG), the source of the earthquake was the Cugenang fault located near the Cimandiri zone with a northwest-southeast direction. Identifying local faults and subsurface structures is vital for developing disaster mitigation, considering the potential risks caused by faults such as seismic damage and landslides.

Detailed research was conducted using the gravity method to determine the location of faults and subsurface geological structures. The gravity data in this research utilized the Global Gravity Model plus (GGMplus) and direct acquisition using a gravimeter. The preliminary study employed GGMplus data because it is accurate, valid, easily accessible, and continuously improved in quality. Satellite data will enchance the accuracy of gravity acquisition data by correcting various factors, such as measurement procedure errors, station position errors, and instrument sensitivity. This study focuses on determining subsurface characteristics based on Earth's gravity field variations due to lateral density differences in direct acquisition and satellite data. First Horizontal Derivative (FHD) and Second Vertical Derivative (SVD) analyses were performed to estimate the accurate location of the fault. 2-D modeling estimated the subsurface structure, which is informative for understanding the complex geological structure[7].

Gravity methods are primarily applied at local to regional scales in geophysical and geological studies. In geophysical and geological analyses, the gravity method

can be used for disaster mitigation such as fault detection and modeling[8–10], mapping natural resource exploration such as geothermal identification and modeling[11–13], volcanic modeling[14,15], and other subsurface reconstructions[16–19]. Satellite data enable the resolution of resource assessment and disaster mitigation challenges over large areas regardless of the weather conditions[20]. Integrating direct acquisition and satellite gravity data is considered more effective, fast, and accurate for disaster mitigation.

2. Materials and method

2.1 Research area

GGMPlus data extraction in this research focused on the Semeru volcano, which is situated geographically within the 49 zone. The elevation range for the satellite gravity area around Semeru volcano spans from 490 meters above sea level (m.a.s.l) to 2590 m.a.s.l, with coordinates stretching from 696327E to 720518E and 9086313N to 9109525N, based on the Universal Transverse Mercator (UTM) system. For this research, the GGMplus data demarcation also encompassed a specific gravity direct acquisition zone within Pronojiwo Sub-district, Lumajang Regency bounded by 713183E to 718514E and 9086084N to 9092525N. The spatial extent of both the satellite and direct acquisition data regions is depicted in Fig. 1.

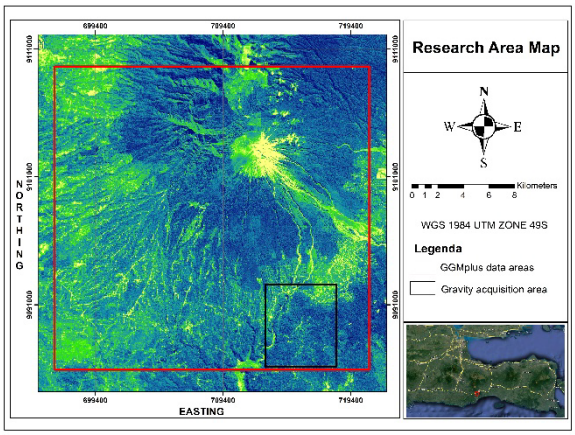

Fig. 1: Research area coverage (this figure was made using DEM SRTM and Google Earth maps). The red rectangle is for the GGMplus, and the purple rectangle is for the direct acquisition area.

An analysis of the geological map reveals that the Semeru volcano straddles the intersection of five geological formations: Wuni, Mandalika, Semeru volcanic deposits, and the volcanic of Jembangan. (Fig.2). These formations consist predominantly of volcanic rock types such as andesitic lava, breccia, and tuff[21–23]. The geological structure that developed in the Pronojiwo was dominated by fault. Notably, the Pronojiwo regions's geological structure is characterized by a prominent fault at the juncture of the Wuni and Mandalika formations, extending in a northwest-southwest direction. This fault line, as identified on the geological map, serves as a crucial reference point for subsequent gravity data collection efforts.

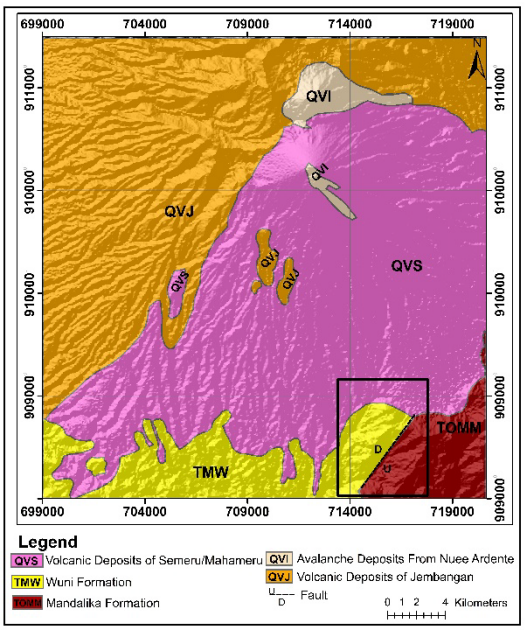

Fig. 2: Geological map of the Semeru, modified based on the geological map[21]. The area in the box covers direct gravity acquisition.

2.2 Data collection and data correction

This research utilized primary (direct acquisition) data and satellite data. The GGMplus satellite data includes latitude, longitude, altitude, and disturbance gravity data, equivalent to gravity readings for free air correction. In contrast, the direct acquisition data, gathered using a Romberg & Lacoste gravimeter model G-1053, underwent initial conversion to milliGal units, followed by a series of corrections. Given the Earth's deviation from a perfectly spherical form, these adjustments must account for geographical variations in gravitational acceleration. In contrast, GGMPlus data offers comprehensive regional insights, and ground-based gravity measurements hone in on localized or residual gravitational anomalies. The integration of these disparate data streams significantly enchances the accuracy of the ensuing subsurface structural analysis.

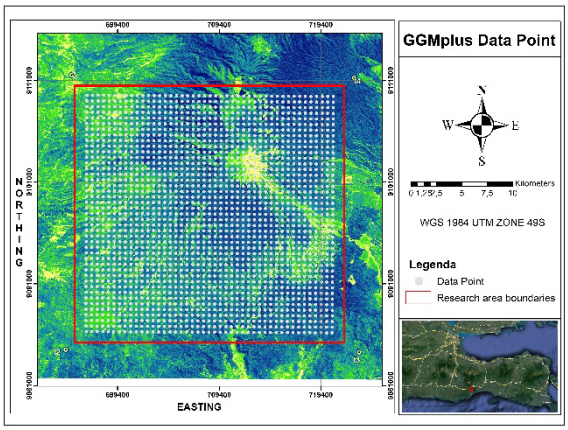

Fig. 3: Research coverage for GGMplus data with 200m space between each point.

The GGMplus satellite gravity data sourced from https://murray-lab.caltech.edu/GGMplus/index.html, obtains the gravity data from multiple sources, including the GRACE (Gravity Recovery and Climate Experiment), GOCE (Gravity field and steady-state Ocean Circulation Explorer), the EGM 2008 (Earth Gravity Model), along with considerations for topographic gravity influences[24]. The precision of this data is notable, offering high-resolution outputs with an estimated granularity of 200 meters[25]. This study utilized 1937 data points, as shown in Fig. 3, arranged in a grid pattern to ensure comprehensive spatial representation [26].

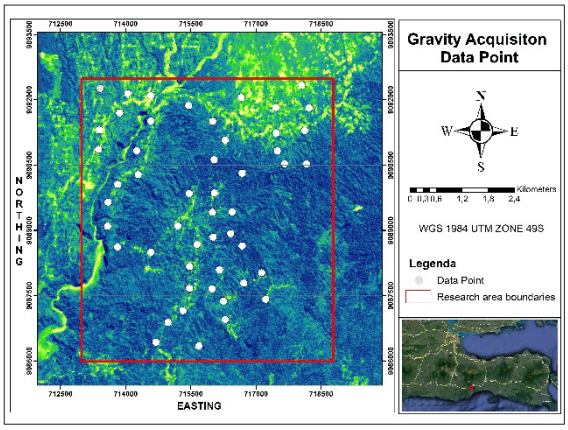

Fig. 4: Acquisition points for direct gravity measurements.

Processing raw gravity data entailed multiple corrective adjustments, including tidal, drift, free air, Bouguer, and terrain. Factors affecting direct gravity values are differences in latitude, topographic conditions, variations in rock mass density, and elevation. Thus, some corrections must be made to remove unnecessary gravity effects[26]. Subsequently, the Parasnis method was applied to determine the local density in the study area employing the CBA (Complete Bouguer Anomaly). The CBA value, reresents the difference between the observed gravity value (g_{obs}) and the theoretical gravity in the reference calculated at a certain point[27]. Gravity data obtained at the observation point cannot be used directly to interpret geological subsurface conditions[28]. Still, they must be corrected to common data by reducing gravity data to the geoid. The topographic surface variations of the area can distort the gravity data. The following equation[28] obtains CBA.

$$CBA = gobs - g\phi + gFA - GB + GT \quad (1)$$

CBA is expressed in mGal, $gobs$ are the value of gravity acceleration at each acquisition point, $g\phi$ is latitude correction, gFA is free air correction, GB is Bouguer correction, and GT is terrain correction.

The Bouguer anomaly is a combined anomaly of the subsurface structure's deep, medium, and shallow anomalies[29,30]. Therefore, a spectrum analysis is needed to segregate regional and residual anomalies, employing an upward continuation filter to isolate these components distinctly. The following process is flat field reduction by converting the Bouguer anomaly values still affected by the topography at the acquisition point to a flat field at a certain height. Reduction of the Bouguer and regional anomalies results in a residual anomaly[31]. Regional anomalies represent deep subsurface geological structures. Residual anomalies indicate the geology above the regional anomalies or are associated with the shallower geological structure. The raw data processing and correction produce CBA values using Microsoft Excel. Then, the CBA anomalies are separated to obtain residual anomalies using Oasis Montaj Software.

2.3 Derivative analysis

Derivative analysis of the gravity data is based on FHD and SVD analysis to indicate the boundaries of geological structures. This analysis aims to show discontinuities in subsurface structures that can indicate faults[29]. The FHD curve's peak adis in pinpointing discontinuities or faults within the subsurface matrix[32,33]. Meanwhile, SVD analysis can describe the residual fault anomalies in shallow structures with zero values between maximum and minimum values. The SVD zero contour anomaly correlated with the maximum point of FHD tends to estimate the fault structure in the study area.

3. Result and discussion

3.1 The gravity anomalies

Based on GGMplus data and direct acquisition gravity data, the Parasnis approach was utilized to determine the study area's average regional rock density. These density values were derived from Bouguer anomalies at varying shallow and deep depths. The computations yielded an average rock density of 2.48 g/cm^3 for the GGMplus satellite gravity data and 2.68 g/cm^3 for the primary gravity measurements.

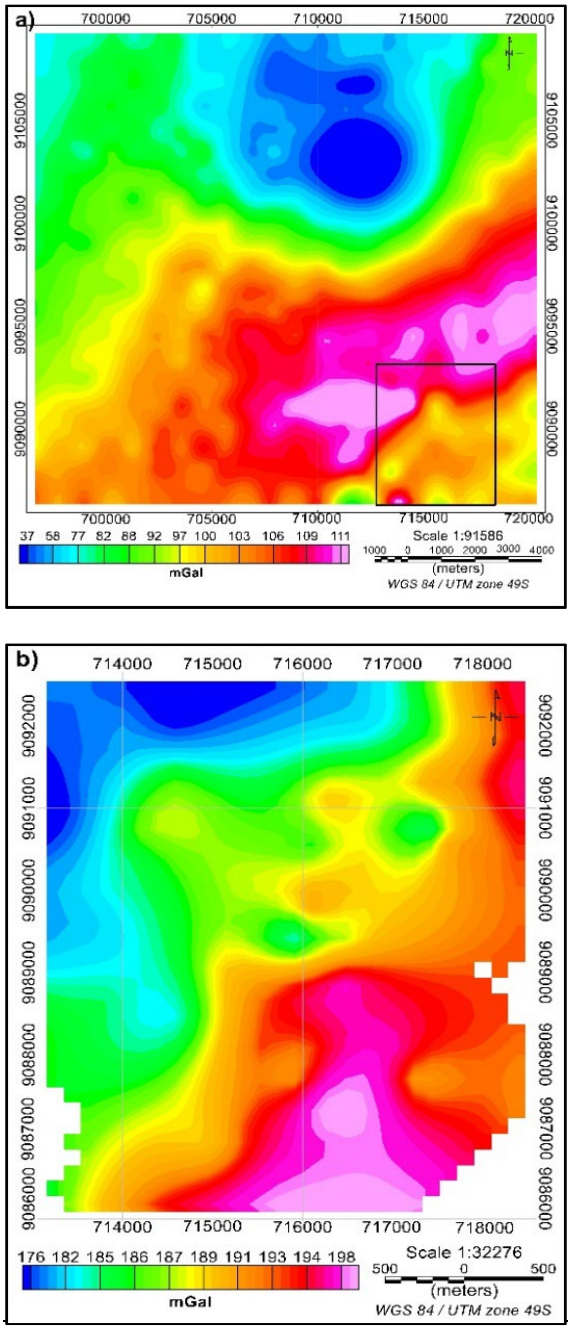

Fig. 5: CBA contour map a) GGMplus data. b) Direct acquisition. Area in the box is the coverage of direct gravity acquisition.

The CBA values, which reflect variations in subsurface rock density, ranged from 37 mGal to 111 mGal for the GGMplus data, as shown in Fig. 5. High anomalies were predominantly located in the eastern to southwestern regions, whereas low anomalies were identified in the northern and some northwestern parts. The elevated anomaly values signify igneous rocks, likely residuals from ancient volcanic activities. Meanwhile, CBA values from direct gravity acquisitions spanned from 176 mGal to 198 mGal, with high-density areas observed in the south, southeast, and northeast. Conversely, lower anomalies were noted in the north, northwest, west, and part of the southwest, suggesting these regions have less dense subsurface structures compared to areas of high anomaly[34].

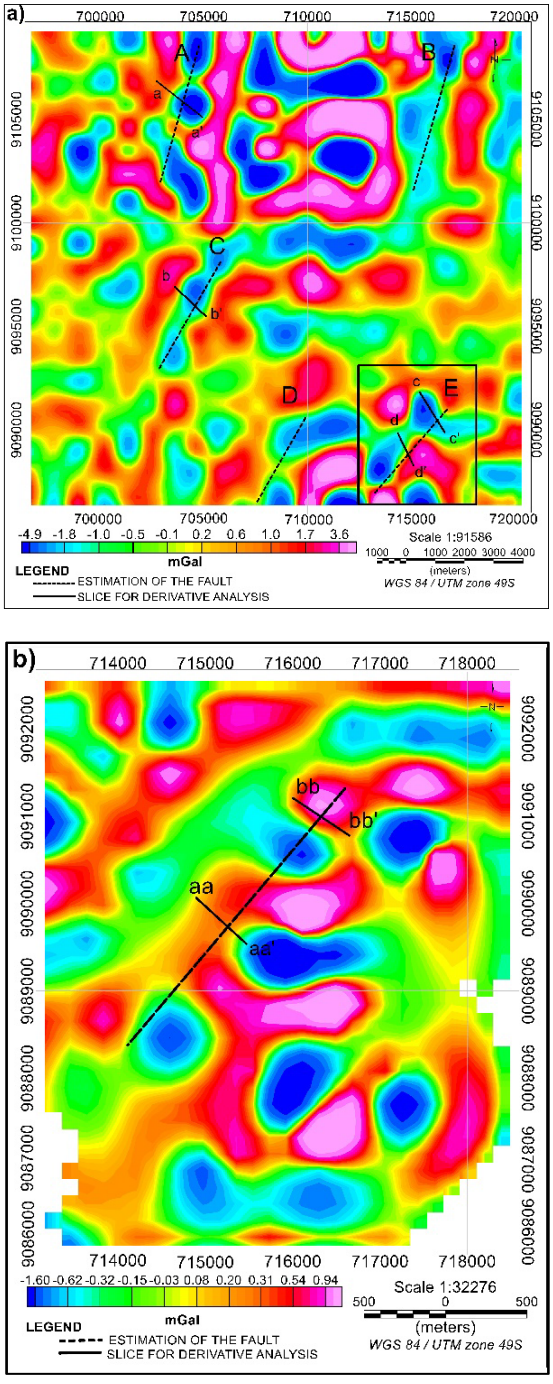

Fig. 6: Residual anomaly contour map a) GGMplus data b) Direct acquisition. The dashed black line is an estimation of the fault zone. The black line is slicing for derivative analysis. Area in the box is coverage of direct gravity acquisition.

The first step in modeling and interpretation of gravity surveys involves eliminating regional anomalies. The process of distinguishing the CBA from regional anomalies facilitates the derivation of residual anomalies[34]. As illustrated in Fig. 6a, the residual anomaly values display a range from -4.91 mGal to 2.88

mGal, with high anomalies stretching from 1.02 mGal to 2.62 mGal and low anomalies from 0.49 mGal to -4.91 mGal.

The residual anomaly derived from the direct gravity data, as depicted in Fig. 6b, varies from -1.6 mGal to 0.94 mGal. The high anomaly values range from 0.31 mGal to 0.94 mGal, whereas the low anomalies vary from -1.5 mGal to -0.32 mGal. The proximity of high and low anomaly areas on the residual map suggests interactions or contacts between different geological structures or anomalies, potentially indicating zones of geological weakness. Such zones are often associated with faults or fractures within the Earth's crust. The analysis identified five potential fault zones within the GGMplus residual anomalies, with one of these estimated fault zones in the southeast corresponding to a fault zone detected in direct acquisition. This fault zone is consistent with the regional geological map, enhancing its credibility. A particular approach in the derivative analysis is needed to confirm this fault zone and identify the presence of deeper geological structures.

3.2 FHD and SVD

Fault detection in this study was analyzed by correlating geological maps (Fig. 2) with the results of derivative analysis performed on gravity data. The research employed a derivative method, effectively identifying shallow sources to highlight anomalies associated with local structures, such as faults. The specific derivative analyses applied were FHD and SVD. These analyses enhance the visibility of fault zones due to the pronounced contrast in anomaly values. In the FHD analysis, areas exhibiting high gravity values, which signify zones of significant rock density contrast[33,35], are depicted in red. Conversely, the SVD analysis helps to pinpoint fault structures based on variations in the gravity anomaly[10], illustrated in white.

The interpretation of residual anomalies involved comparing the peak values in FHD and the contrasting patterns in SVD to sketch a provisional outline of fault structures. This step was followed by delineating four fault structures oriented perpendicularly to the identified faults to confirm their existence. On the GGMplus derivative map, five potential fault structures labeled ABCDE were identified. Cross-referencing with the geological map (see Fig. 2) reveals that only one fault, directed southeast, aligns with the D structure identified in the geological and derivative acquisition data.

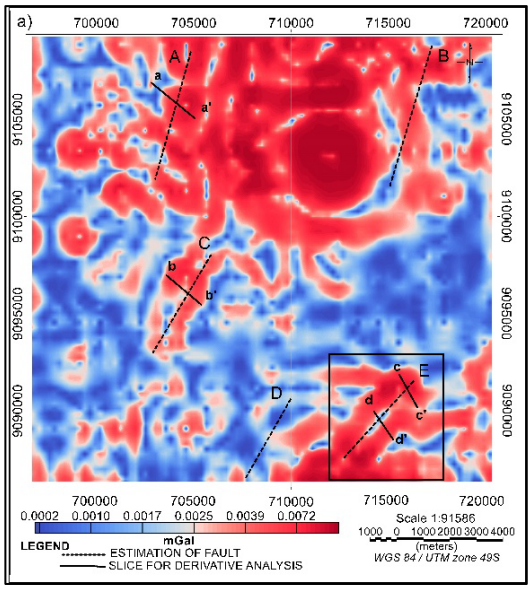

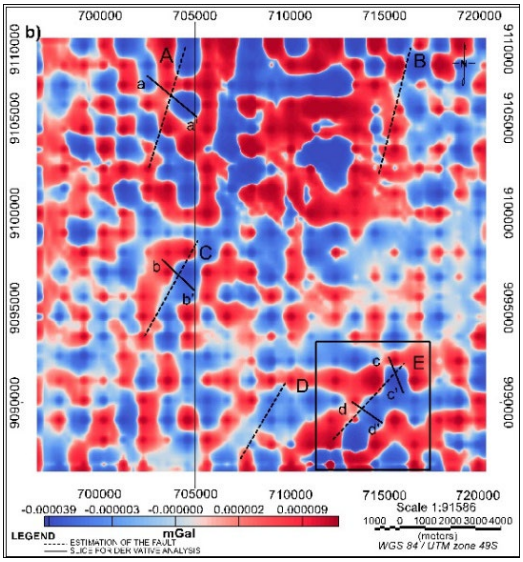

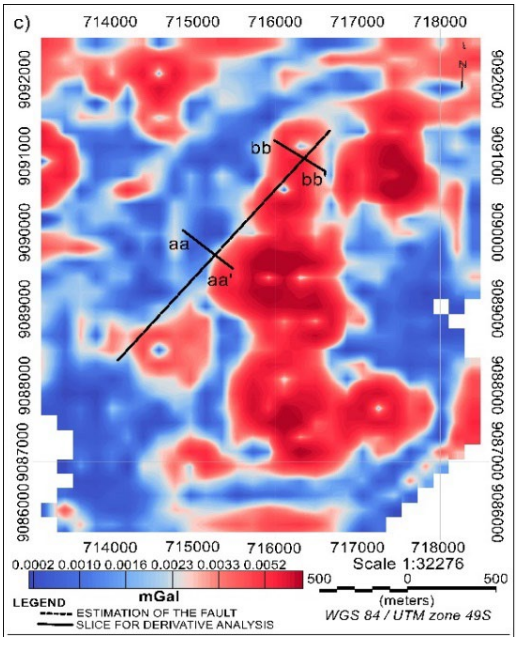

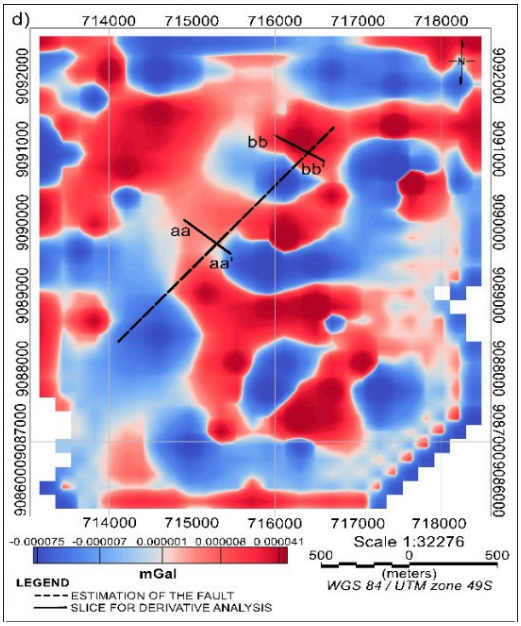

Fig. 7: Map view of FHD and SVD. (a) FHD anomaly map of GGMplus data. (b) SVD anomaly map of GGMplus data. (c) FHD anomaly map of gravity acquisition data. (d) SVD anomaly map of gravity acquisition data.

Two cross-sectional analyses (c-c' and d-d') were conducted to substantiate the existence of the D fault. Additionally, one cross-section each was performed for faults A and C (a-a' and b-b', respectively), representing areas where the derivative analysis suggested faults not confirmed by the geological map. The same delineation procedure was applied to the direct acquisition fault zone corresponding with the D GGMplus fault, ensuring the cross-sections (aa-aa' and bb-bb') were analyzed at identical coordinates. The subsequent plotting of residual anomaly delineations (refer to Fig. 6) alongside FHD and SVD analyses (see Fig. 7) generated three graphical representations that corroborate the presence of these fault structures, as detailed in Fig. 8.

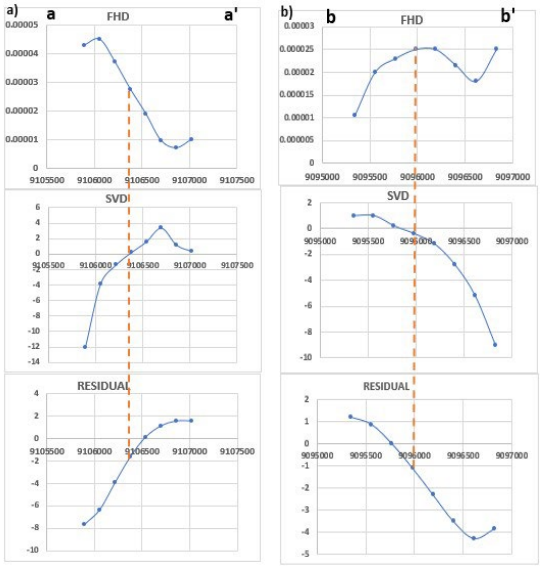

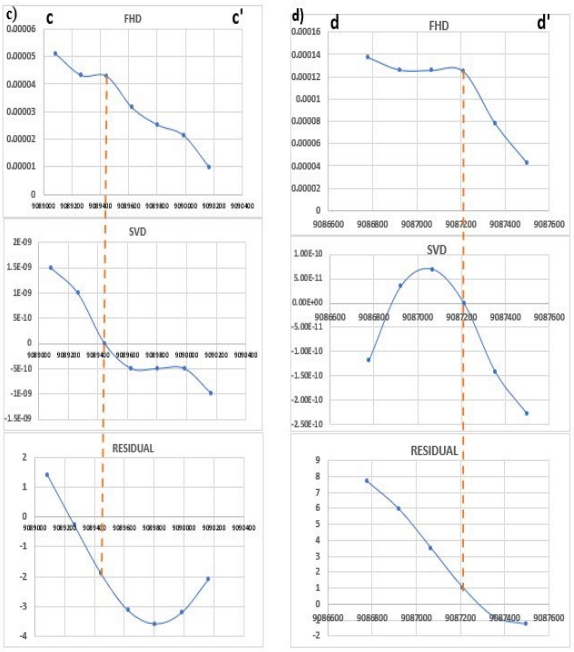

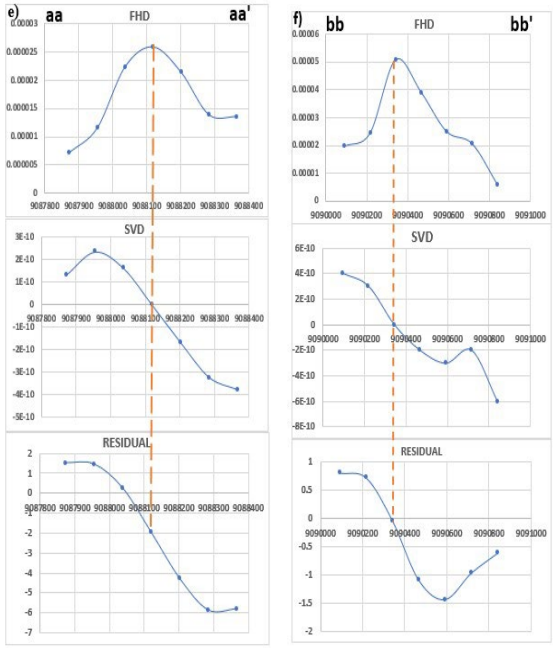

Fig. 8: Slicing line graph: a). Slicing a-a' chart of GGMplus data. b) Slicing b-b' chart of GGMplus data, c). Slicing c-c' chart of GGMplus data, d) Slicing d-d' chart of gravity GGMplus data. e) Slicing aa-aa' chart of acquisition data.f) Slicing bb-bb' chart of acquisition data.

The slicing results shown in Fig. 8 demonstrate that where the slicing line intersects a significant density contrast boundary, the FHD curve reaches its maximum value, and the SVD curve drops to zero. Straight lines on the FHD and SVD curves illustrate the correlation between high and low anomalies, suggesting a boundary contact along the slicing path, interpreted as a fault[36]. Figures 8a) and 8b) present the derivative analysis for the suspected faults A and C. Notably, the maximum FHD value aligns with a non-zero SVD value in these regions,

yet no corresponding faults are indicated on the geological map. Consequently, based on the principles of derivative analysis and its correlation with geological mapping, faults A and C are not confirmed as actual faults. Similarly, the lack of geological map evidence for the suspected faults B and D is not confirmed and thus are not identified as faults.

The results of slicing the D fault of GGMplus data are presented in graphs 8c and 8d, while the derivative analysis of direct acquisition is shown in graphs 8e and 8f. These graphs demonstrate a maximum in FHD and a zero value in the correlated SVD, indicating that fault D constitutes a fault structure. The point where SVD equals zero corresponds with a density contrast transition, identifying the source of the subsurface anomaly[37]. This is also confirmed by the geological map from the Geological Research and Development Centre [21]. The suspected fault D in the Pronojiwo sub-district is confirmed by meeting the derivative analysis criteria and referencing the geological map.

3.3 Subsurface Model

Based on the occurrence of the D fault and potential fault of direct acquisition, a 2-D model of the subsurface structure will be created using the derivative analysis slices d-d' from GGMplus gravity data and aa-aa' from direct acquisition data (refer to Fig. 7). This model will include FHD and SVD curves to enhance the visualization of the fault target, aligning the predicted fault location with the peak of the FHD curve, which correlates with the zero point on the SVD curve. The density values inform the geological structure depicted in the 2-D model of igneous and sedimentary rocks in the study area[34].

The d-d' slice in northwest-southeast orientation, as shown in Fig. 9 and extending 800 meters in length, shows a modeling error of 2,873 mGal, which is associated with the computations made in the software. This model comprises three rock formations, categorized based on their density distributions and the geological context of the study area, with densities ranging from 2.9 g/cm³ to 2 g/cm³. The uppermost formation, rendered in pink, is classified as tuff with a 2 g/cm³ density. This tuff formation, part of the Semeru volcanic formation, extends from 200 m to 800 meters. The intermediate formation, depicted in yellow, is identified as breccia with a 2.67 g/cm³ density. In the eastern section, this breccia formation ranges from 300 m to 800 m deep, whereas in the western section, it is found between 450 m and 650 m deep, suggesting potential uplift of the substrate in the west. The deepest formation is inferred to be andesitic lava, noted for its higher density of 2.9 g/cm³ and commencing at a depth of 500 m.

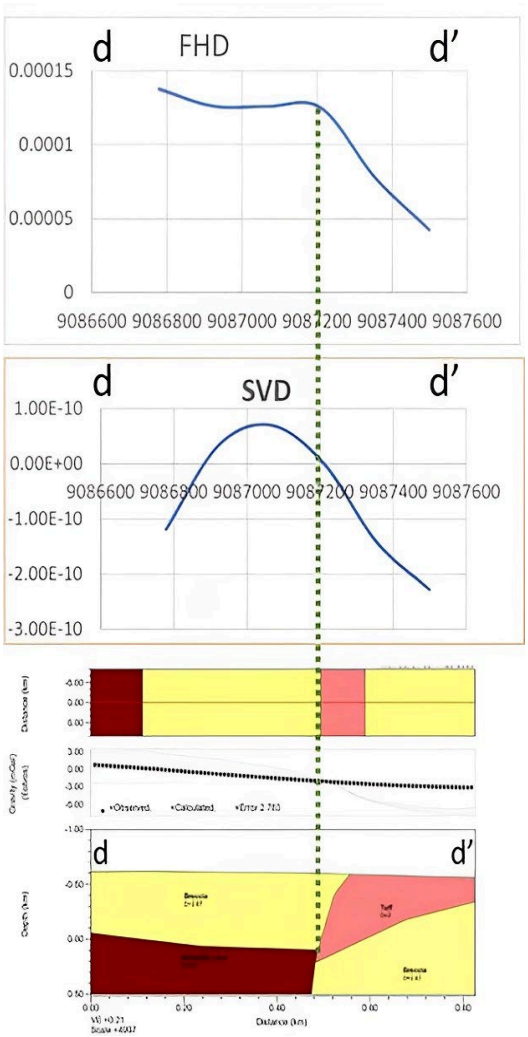

Fig. 9: 2-D modeling of d-d' slicing GGMplus data.

The cross-section model from the aa-aa' slicing, displayed in Fig. 10 and oriented in a northwest-southeast direction, presents density values ranging from 2.9 g/cm³ to 2 g/cm³ over 800 meters. This aa-aa' model aligns with the d-d' slice, encapsulating three stratified rock formations. Low anomaly values are attributed to the tuff and breccia formations, which are components of the younger Semeru volcanic formations. These low-density volcanic fallout deposits impact the correlation between the lithological properties and the observed low gravity anomalies within the volcanic region[38]. Conversely, the high anomaly values are likely due to denser igneous formations, specifically andesitic lava[39]. An error margin of approximately 1,473 mGal in the aa-aa' model necessitates the correlation of this 2-D modeling with both GGMPlus and direct acquisition gravity data to ensure consistency and accuracy.

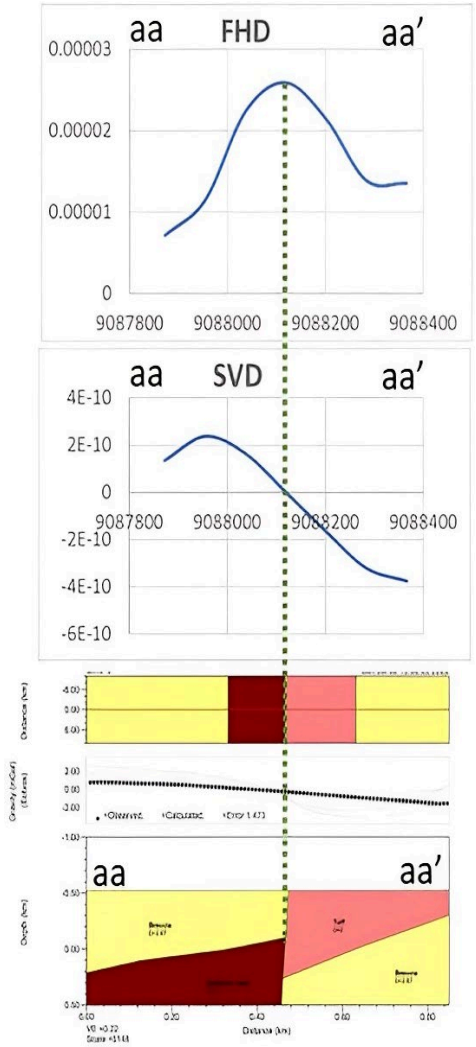

Fig. 10: 2-D modeling of aa-aa' slicing gravity acquisition data.

Based on Figures 9 and 10, the First Horizontal Derivative (FHD), Second Vertical Derivative (SVD), and 2-D modeling curves collectively indicate the locations of faults, which are oriented in the northeast-southwest direction. These faults result in the downward displacement of the western rock block (acting as the footwall) relative to the eastern rock block (acting as the hanging wall) along the fault plane. This interpretation is supported by data from the geological and morphological map of Semeru Volcano Piedmont, composed of Alluvial and Laharic Piedmont[40]. Furthermore, the interaction of Semeru/Mahameru eruption deposits and remnants of lava with the older geological layers, such as the Oligocene-Miocene Tuff and the Andesite Formation, delineates normal fault boundaries. These faults are attributed to vertical compression and the uplifting of rock formations, processes associated with the subduction zone located to the south of the volcano[39].

4. Conclusion

The gravity analysis indicates the presence of a subsurface fault structure beneath the Pronojiwo sub-district. The residual anomaly values range from -4.9 mGal to 3.6 mGal for GGMplus data and from -1.6 mGal to 0.94 mGal for direct acquisition. The contrast between high and low anomalies, illustrated on the residual maps, delineates an estimated fault zone. The derivative analysis confirms this fault structure, as shown by the alignment of high and low anomalies along the slicing path and the intersection of the FHD curve's peak with the SVD curve's zero value. The FHD and SVD analyses also suggest that the fault orientation is predominantly in the northeast-southwest direction.

The analysis and modeling results, integrating satellite gravity data and direct observations, reveal a consistent anomaly pattern, identifying three principal subsurface formations: andesitic lava, breccia, and tuff. These determinations are based on comparisons of regional geological maps and rock density data.

Acknowledgements

The authors are grateful to Brawijaya Volcano and Geothermal Research Center (BRAVO GRC) of Brawijaya, Malang, East Java for all supports and valuable thoughts. This research was partially funded by Institution of Research and Community Services of Brawijaya University (LPPM-UB) on a Leading Research Grants Program under contract number 612.39/UN10.C20/2023 and Grants for Professor's Research of Faculty of Mathematics and Natural Sciences, Brawijaya University Malang under contract number: 4158.10/UN10.F09/PN/2023. Authors also thank the Bruce Murray Laboratory for the data used in this study which is obtained from a Global Gravity Model plus (GGMplus) satellite by California Institute of Technology (https://murray-lab.caltech.edu/GGMplus/index.html), Division of Geological & Planetary Sciences, and the USGS that has provided the SRTM DEM data for this research.

References

1) A. Susilo, Sunaryo, F. Fitriah, and Sarjiyana, "Fault analysis in pohgajih village, blitar, indonesia using resistivity method for hazard risk reduction," *Int. J. GEOMATE*, **14** (*41*) 111–118 (2018). doi:10.21660/2018.41.87552.
2) X.L. Wei, C.X. Zhang, S.W. Kim, K.L. Jing, Y.J. Wang, S. Xu, and Z.Z. Xie, "Seismic fault detection using convolutional neural networks with focal loss," *Comput. Geosci.*, **158** (*1*) 1–15 (2022). doi:10.1016/j.cageo.2021.104968.
3) C. Gasston, J.M. Lindsay, J.D. Eccles, M. Brook, M. Hill, and J. Kenny, "A geophysical and geomorphological investigation of large-offset normal faulting in beachlands, auckland," *New Zeal. J. Geol. Geophys.*, **64** (*1*) 37–48 (2021).

doi:10.1080/00288306.2020.1734032.

4) F. Muttaqy, A.D. Nugraha, J. Mori, N.T. Puspito, P. Supendi, and S. Rohadi, "Seismic imaging of lithospheric structure beneath central-east java region, indonesia: relation to recent earthquakes," *Front. Earth Sci.*, **10** (*January*) 1–15 (2022). doi:10.3389/feart.2022.756806.
5) A. Susilo, and Z. Adnan, "Probabilistic seismic hazard analysis of east java region , indonesia," *Int. J. Comput. Electr. Eng.*, **5** (*3*) 341–344 (2013). doi:10.7763/IJCEE.2013.V5.728.
6) W.D. Aryani, S. Sutisna, Lasmono, P. Widodo, and H.J.R. Saragih, "The strategy of housing rehabilitation and reconstruction after 2022 earthquake in cianjur, west java, indonesia," *Int. J. Humanit. Educ. Soc. Sci.*, **2** (*5*) 1705–1711 (2023).
7) H. Kausarian, Lady Redyafry, J.T.S. Sumantyo, A. Suryadi, and M.Z. Lubis, "Structural analysis of the central sumatra basin using geological mapping and landsat 8 oli/tirs c2 l1 data," *Evergreen*, **10** (*2*) 792–804 (2023). doi:10.5109/6792830.
8) Y. Hiramatsu, A. Sawada, W. Kobayashi, S. Ishida, and M. Hamada, "Gravity gradient tensor analysis to an active fault: a case study at the togi-gawa nangan fault, noto peninsula, central japan," *Earth, Planets Sp.*, **71** (*1*) (2019). doi:10.1186/s40623-019-1088-5.
9) W.M.S. Al-Khafaji, "Gravity field interpretation for major fault depth detection in a region located sw-qa'im / iraq," *Baghdad Sci. J.*, **14** (*3*) 625–636 (2017). doi:10.21123/bsj.2017.14.3.0625.
10) M. Yanis, F. Abdullah, N. Zaini, and N. Ismail, "The northernmost part of the great sumatran fault map and images derived from gravity anomaly," *Acta Geophys.*, **69** (*3*) 795–807 (2021). doi:10.1007/s11600-021-00567-9.
11) N.A.G. Lestari, S. Maryanto, and D.R. Santoso, "Derivative Analysis for Estimating Subsurface Structures in the Kawi-Songgoriti Geothermal Area," in: 3rd Int. Conf. Sci. Math. Environ. Educ. AIP Conf. Proc., 2023: pp. 1–11. doi:10.1063/5.0106820.
12) J.B. Witter, D.L. Siler, J.E. Faulds, and N.H. Hinz, "3D geophysical inversion modeling of gravity data to test the 3d geologic model of the bradys geothermal area, nevada, usa," *Geotherm. Energy*, **4** (*1*) (2016). doi:10.1186/s40517-016-0056-6.
13) J. d'Amour Uwiduhaye, H. Mizunaga, and H. Saibi, "Survey.pdf," *J. African Earth Sci.*, **2018** (*139*) 184–192 (2017).
14) J. Gottsmann, A.G. Camacho, J. Martí, L. Wooller, J. Fernández, A. García, and H. Rymer, "Shallow structure beneath the central volcanic complex of tenerife from new gravity data: implications for its evolution and recent reactivation," *Phys. Earth Planet. Inter.*, **168** (*3–4*) 212–230 (2008). doi:10.1016/j.pepi.2008.06.020.
15) E. Aboud, A. Shareef, F.A. Alqahtani, and S. Mogren, "Using a 3d gravity inversion technique to image the subsurface density structure in the lunayyir volcanic field, saudi arabia," *J. Asian Earth Sci.*, **161** (*May*) 14–24 (2018). doi:10.1016/j.jseaes.2018.05.002.
16) J. Urrutia-Fucugauchi, L. Pérez-Cruz, O. Alvarado-Velázquez, G. Álvarez-Solís, D. Valdés-Casillas, Y. Atala-Muñoz, and M. Díaz-Flores, "Gravity survey of the mesoamerican cuicuilco archaeological site, southern basin of mexico," *Arqueol. Iberoam.*, **42** 3–8 (2019). doi:10.5281/zenodo.3477608.
17) A. Mohamed, and J. Gonçalvès, "Hydro-geophysical monitoring of the north western sahara aquifer system's groundwater resources using gravity data," *J. African Earth Sci.*, **178** (*July 2020*) (2021). doi:10.1016/j.jafrearsci.2021.104188.
18) M. Albayrak, C. Hirt, S. Guillaume, K. Halicioglu, M.T. Özlüdemir, and C.K. Shum, "Quality assessment of global gravity field models in coastal zones: a case study using astrogeodetic vertical deflections in istanbul, turkey," *Stud. Geophys. Geod.*, **64** (*3*) 306–329 (2020). doi:10.1007/s11200-019-0591-2.
19) S. Singh, S.K. Singh, R. Kumar, A. Shrama, and S. Kanga, "Finding alternative to river sand in building construction," *Evergreen*, **9** (*4*) 973–992 (2022). doi:10.5109/6625713.
20) A. Yussupov, and R.Z. Suleimenova, "Use of remote sensing data for environmental monitoring of desertification," *Evergreen*, **10** (*1*) 300–307 (2023). doi:10.5109/6781080.
21) Sujanto, Hadisantono R, Kusnama, C. R, and B. R, "GEOLOGIC MAP OF THE TUREN QUADRANGLE, JAWA," Geological Research and Development Centre, Bandung, 1992.
22) Sutawidjaja I.S., Wahyudin, and E. D., Kusdinar, "Geological Map of Semeru Volcano, East Java," Volcanological Survey of Indonesia, Bandung, Indonesia, 1996.
23) J.C. Thouret, F. Lavigne, H. Suwa, B. Sukatja, and Surono, "Volcanic hazards at mount semeru, east java (indonesia), with emphasis on lahars," *Bull. Volcanol.*, **70** (*2*) 221–244 (2007). doi:10.1007/s00445-007-0133-6.
24) Supriyadi, V. Soraya, A. Suprianto, and N. Priyantari, "Identification of blawan-ijen fault based on ggmplus gravity data using second vertical derivative (svd) analysis," *3rd Int. Conf. Phys. Instrum. Adv. Mater. 2021*, **040005** (*2663*) (2022). doi:https://doi.org/10.1063/5.0108055.
25) C. Hirt, S. Claessens, T. Fecher, M. Kuhn, R. Pail, and M. Rexer, "New ultrahigh-resolution picture of earth's gravity field," *Geophys. Res. Lett.*, **40** (*16*) 4279–4283 (2013). doi:10.1002/grl.50838.
26) M.F.R. Hasan, A. Susilo, E.A. Suryo, P.A.M. Agung, M.H. Idmi, D.A. Suaidi, and F. Aprilia, "Iraqi geological journal," **57** (*1A*) 159–168 (2024). doi:10.46717/igj.57.1A.13ms-2024-1-24.
27) M. Justia, M.F.H. Hiola, and N.B. Febryana S,

"Gravity anomaly to identify walanae fault using second vertical derivative method," *J. Phys. Theor. Appl.*, **2** (*1*) 34 (2018). doi:10.20961/jphystheor-appl.v2i1.29008.

28) J.M. Reynolds, "Development of a mems rate sensor," 2nd Editio, John Wiley & Sons, Ltd, 2006.
29) R.J. Blakely, "Potential theory in gravity and magnetic applications," Cambridge university press, 1996.
30) S.H. Siombone, S. Maryanto, and . Wiyono, "Bouguer anomaly of geothermal reservoir at tiris area, probolinggo, east java, indonesia," *J. Geogr. Environ. Earth Sci. Int.*, **25** (*9*) 1–18 (2021). doi:10.9734/jgeesi/2021/v25i930304.
31) H. Kebede, A. Alemu, and S. Fisseha, "Upward continuation and polynomial trend analysis as a gravity data decomposition, case study at ziway-shala basin, central main ethiopian rift," *Heliyon*, **6** (*1*) e03292 (2020). doi:10.1016/j.heliyon.2020.e03292.
32) A. Barkah, and Y. Daud, "Identification of structural geologyat the tangkuban parahu geothermal area, west java based on remote sensing and gravity data," *AIP Conf. Proc.*, **2320** (2021). doi:10.1063/5.0038809.
33) M.S. Rosid, S. Nursarifa, and A. Riyanto, "Identification of geological structures in sigi regency, central sulawesi based on derivative analysis of gravity data," *Int. J. GEOMATE*, **24** (*103*) 26–33 (2023). doi:10.21660/2023.103.3426.
34) W.M. Telford, W.M. Telford, L.P. Geldart, and R.E. Sheriff, "Applied geophysics," Cambridge university press, USA, 1990.
35) M.S. Rosid, and C.B. Sawaswati, "Implementation 3d inversion of gravity data to identify potential hydrocarbon reservoir zones in west timor basin," *Sains Malaysiana*, **49** (*9*) 2065–2072 (2020).
36) P. Sumintadireja, D. Dahrin, and H. Grandis, "A note on the use of the second vertical derivative (svd) of gravity data with reference to indonesian cases," *J. Eng. Technol. Sci.*, **50** (*1*) 127–139 (2018). doi:10.5614/j.eng.technol.sci.2018.50.1.9.
37) M.S. Rosid, "Determining Fault Structure using First Horizontal Derivative (FHD) and Horizontal Vertical Diagonal Maxima (HVDM) Method: a Comparative Study," in: Int. Symp. Curr. Prog. Math. Sci., 2017: pp. 1–10. doi:10.1063/1.4991275.
38) E. Thiel, "CORRELATION of gravity anomalies with the keweenawan geology of wisconsin and minnesota," *Bull. Geol. Soc. Am.*, **67** (*11*) 1079–1100 (1956).
39) A. Solikhin, J. Thouret, A. Gupta, A.J.L. Harris, and S. Chin, "Geomorphology geology , tectonics , and the 2002 – 2003 eruption of the semeru volcano , indonesia : interpreted from high-spatial resolution satellite imagery," *Geomorphology*, **138** (*1*) 364–379 (2012). doi:10.1016/j.geomorph.2011.10.001.
40) Z. Kassouk, J. Thouret, A. Gupta, A. Solikhin, and S. Chin, "Object-oriented classification of a high-spatial resolution spot5 image for mapping geology and landforms of active volcanoes : semeru case study , indonesia," *Geomorphology*, **221** 18–33 (2014). doi:10.1016/j.geomorph.2014.04.022.